

University of Groningen

Temperature-independent giant dielectric response in transitional BaTiO₃ thin films

Everhardt, Arnoud S.; Denneulin, Thibaud; Gruenebohm, Anna; Shao, Yu-Tsun; Ondrejko, Petr; Zhou, Silang; Domingo, Neus; Catalan, Gustau; Hlinka, Jiri; Zuo, Jian-Min

Published in:
Applied physics reviews

DOI:
[10.1063/1.5122954](https://doi.org/10.1063/1.5122954)

IMPORTANT NOTE: You are advised to consult the publisher's version (publisher's PDF) if you wish to cite from it. Please check the document version below.

Document Version
Publisher's PDF, also known as Version of record

Publication date:
2020

[Link to publication in University of Groningen/UMCG research database](#)

Citation for published version (APA):

Everhardt, A. S., Denneulin, T., Gruenebohm, A., Shao, Y-T., Ondrejko, P., Zhou, S., Domingo, N., Catalan, G., Hlinka, J., Zuo, J-M., Matzen, S., & Noheda, B. (2020). Temperature-independent giant dielectric response in transitional BaTiO₃ thin films. *Applied physics reviews*, 7(1), [011402]. <https://doi.org/10.1063/1.5122954>

Copyright

Other than for strictly personal use, it is not permitted to download or to forward/distribute the text or part of it without the consent of the author(s) and/or copyright holder(s), unless the work is under an open content license (like Creative Commons).

The publication may also be distributed here under the terms of Article 25fa of the Dutch Copyright Act, indicated by the "Taverne" license. More information can be found on the University of Groningen website: <https://www.rug.nl/library/open-access/self-archiving-pure/taverne-amendment>.

Take-down policy







If you believe that this document breaches copyright please contact us providing details, and we will remove access to the work immediately and investigate your claim.

Downloaded from the University of Groningen/UMCG research database (Pure): <http://www.rug.nl/research/portal>. For technical reasons the number of authors shown on this cover page is limited to 10 maximum.


Temperature-independent giant dielectric response in transitional BaTiO₃ thin films

Cite as: Appl. Phys. Rev. **7**, 011402 (2020); <https://doi.org/10.1063/1.5122954>

Submitted: 02 August 2019 . Accepted: 17 December 2019 . Published Online: 21 January 2020

Arnoud S. Everhardt , Thibaud Denneulin, Anna Grünebohm , Yu-Tsun Shao, Petr Ondrejko, Silang Zhou, Neus Domingo , Gustau Catalan , Jiří Hlinka , Jian-Min Zuo, Sylvia Matzen, and Beatriz Noheda 

COLLECTIONS

 This paper was selected as Featured



View Online



Export Citation



CrossMark

ARTICLES YOU MAY BE INTERESTED IN

[Research suggests a new class of ferroelectric materials](#)

SciLight **2020**, 041101 (2020); <https://doi.org/10.1063/10.0000632>

[Tailoring magnetic order via atomically stacking 3d/5d electrons to achieve high-performance spintronic devices](#)

Applied Physics Reviews **7**, 011401 (2020); <https://doi.org/10.1063/1.5124373>

[A magnetic phase diagram for nanoscale epitaxial BiFeO₃ films](#)

Applied Physics Reviews **6**, 041404 (2019); <https://doi.org/10.1063/1.5113530>



Applied Physics Reviews

Submit your original research today!

LEARN MORE >>>

Journal
Impact Factor
12.750



Temperature-independent giant dielectric response in transitional BaTiO₃ thin films



Cite as: Appl. Phys. Rev. **7**, 011402 (2020); doi: [10.1063/1.5122954](https://doi.org/10.1063/1.5122954)

Submitted: 2 August 2019 · Accepted: 17 December 2019 ·

Published Online: 21 January 2020 · Publisher error corrected 14 February 2020



Arnoud S. Everhardt,^{1,a)} Thibaud Denneulin,^{2,3} Anna Grünebohm,⁴ Yu-Tsun Shao,⁵ Petr Ondrejkojic,⁶ Silang Zhou,¹ Neus Domingo,⁷ Gustau Catalan,^{7,8} Jiří Hlinka,⁶ Jian-Min Zuo,⁵ Sylvia Matzen,⁹ and Beatriz Noheda^{1,10,b)}

AFFILIATIONS

¹Zernike Institute for Advanced Materials, University of Groningen, 9747 AG Groningen, The Netherlands

²CEMES-CNRS, F-31055 Toulouse Cedex 4, France

³Ernst Ruska-Centre for Microscopy and Spectroscopy with Electrons (ER-C), Forschungszentrum Jülich, 52425 Jülich, Germany

⁴ICAMS, Ruhr-Universität Bochum, 44801 Bochum, Germany

⁵Department of Materials Science and Engineering, University of Illinois, Urbana, Illinois 61801, USA

⁶Institute of Physics of the Czech Academy of Sciences, Na Slovance 2, 18221 Praha 8, Czech Republic

⁷Catalan Institute of Nanoscience and Nanotechnology (ICN2), CSIC, Barcelona Institute of Science and Technology Campus, Universitat Autònoma de Barcelona, Bellaterra, 08193 Barcelona, Spain

⁸ICREA, 08193 Barcelona, Spain

⁹Center for Nanoscience and Nanotechnology, UMR CNRS-Université Paris-Sud, Université Paris-Saclay, Avenue de la Vauve, 91120 Palaiseau, France

¹⁰Groningen Cognitive Systems and Materials Centre (CogniGron), University of Groningen, 9747 AG Groningen, The Netherlands

^{a)}Present address: Materials Science Division, Lawrence Berkeley National Laboratory, Berkeley, CA 94720, USA.

^{b)}E-mail: b.noheda@rug.nl

ABSTRACT

Ferroelectric materials exhibit the largest dielectric permittivities and piezoelectric responses in nature, making them invaluable in applications from supercapacitors or sensors to actuators or electromechanical transducers. The origin of this behavior is their proximity to phase transitions. However, the largest possible responses are most often not utilized due to the impracticality of using temperature as a control parameter and to operate at phase transitions. This has motivated the design of solid solutions with morphotropic phase boundaries between different polar phases that are tuned by composition and that are weakly dependent on temperature. Thus far, the best piezoelectrics have been achieved in materials with intermediate (bridging or adaptive) phases. But so far, complex chemistry or an intricate microstructure has been required to achieve temperature-independent phase-transition boundaries. Here, we report such a temperature-independent bridging state in thin films of chemically simple BaTiO₃. A coexistence among tetragonal, orthorhombic, and their bridging low-symmetry phases are shown to induce continuous vertical polarization rotation, which recreates a smear in-transition state and leads to a giant temperature-independent dielectric response. The current material contains a ferroelectric state that is distinct from those at morphotropic phase boundaries and cannot be considered as ferroelectric crystals. We believe that other materials can be engineered in a similar way to contain a ferroelectric state with gradual change of structure, forming a class of transitional ferroelectrics. Similar mechanisms could be utilized in other materials to design low-power ferroelectrics, piezoelectrics, dielectrics, or shape-memory alloys, as well as efficient electro- and magnetocalorics.

© 2020 Author(s). All article content, except where otherwise noted, is licensed under a Creative Commons Attribution (CC BY) license (<http://creativecommons.org/licenses/by/4.0/>). <https://doi.org/10.1063/1.5122954>

Phase transitions (PTs) are among the most interesting and ubiquitous phenomena in nature.¹ In materials science, they are responsible for the technological impact of ferromagnets, ferroelectrics,² shape-memory alloys, or memristors.³ PTs are associated with desirably large,

nonlinear changes in the order parameters (magnetization, polarization, resistance, etc.) and susceptibilities. However, they are often also associated with energy losses, resulting from the cost of nucleating one phase into the other.

Ferroelectrics are an interesting class of materials due to their spontaneous polarization and large responses to external stimuli (electric field or stress), which characterizes them with the largest existing capacitances and electromechanical responses. Operating a ferroelectric near its transition temperature T_C ^{4–9} induces flattening of the energy potential and maximizes its dielectric and piezoelectric responses. However, the drawback is poor temperature stability. A way around this problem has been found by engineering phase boundaries between two polar phases via changes of a parameter that is robustly fixed during the lifetime of the device, such as composition. This approach requires careful tuning of the chemistry in order to obtain phase boundaries that are temperature-independent, that is parallel to the temperature axis in the temperature-composition phase diagram (known as morphotropic phase boundaries, MPB). This is the case of PZT or PMN-PT,⁵ the materials with the best performance. These are still used in most applications despite their lead content, as most alternatives lack the required temperature stability. More recently, compositional gradients have been utilized to achieve large dielectric responses,¹⁰ again requiring a careful control of the composition. Early pioneering work^{11–15} has established that the origin of the large piezoelectric and dielectric responses around MPBs is the polarization rotation that takes place in low symmetry monoclinic or triclinic phases present at MPBs. In addition, because the MPB features and the low-symmetry phases are a result of the need for elastic matching of the different phases coexisting at the MPB,¹⁶ these exceptional properties do not always survive when the material is grown in thin film form, under demanding boundary conditions.

A similar phenomenon has been observed in BaTiO₃, at a so-called Thermotropic Phase Boundary,¹⁷ in between the tetragonal and orthorhombic phases, where a bridging low-symmetry phase can be found locally in a certain temperature regime around the phase transition. MPB-like features are also reported in BiFeO₃ thin films under strain, where two phases coexist and form a complex nanodomain structure with a lowered symmetry, polar rotation, and enhanced piezoelectric response.¹⁸ However, in these chemically simple compounds the temperature stability of the large responses has not been demonstrated.

In this paper, we report a mechanism that leads to huge and temperature-independent dielectric responses and large piezoelectric responses in lead-free, ferroelectric films of the classical ferroelectric BaTiO₃. In these films, the proximity to different stability minima renders evolving polar domain configurations within the same film, including intermediate bridging phases that support rotation of polarization. These materials cannot be considered ferroelectric crystals, and we propose the term transitional ferroelectrics to emphasize their unique responses.

EFFECT OF BOUNDARY CONDITIONS ON THE POLAR STATE AND SWITCHING OF BaTiO₃

BaTiO₃ thin films with thicknesses between 30 and 300 nm have been grown on NdScO₃ substrates with SrRuO₃ bottom (and optionally also top) electrodes by pulsed laser deposition. (Details can be found in the Methods section in Note S1 in the [supplementary material](#).) Two different domain configurations had been reported to exist in these films close to room temperature.¹⁹ One of the

structures is the well-known *a/c* multidomain phase, consisting of alternating in-plane (*a*-domain) and out-of-plane (*c*-domain) polarized regions, common in tetragonal thin films; the second structure was described as resembling the 90° in-plane domain configuration (*a*₁/*a*₂) with an additional weak out-of-plane component. However, the observed contrast in the Piezoelectric Force Microscopy (PFM) images was unusually weak for a strongly polar material, such as BaTiO₃, and the details of this complex domain structure and phase diagram are still under debate.^{19–23}

Dark-field Transmission Electron Microscopy (TEM) [Fig. 1(a)] has been performed on these BaTiO₃ films to shed light on the details of the domain configurations throughout the film. Due to dynamical diffraction, the variations of contrast in the dark-field TEM are related to variations of the ferroelectric polarization along the direction of the selected diffracted beam.^{24,25} We observed a strong dependence of the domain orientations both on thickness and on electrical boundary conditions. Using quasisymmetric and thick enough (above 10 nm) electrodes, the films develop a 180° domain wall close to the center of the films, parallel to the film/electrode interfaces (hereafter referred to as “horizontal” direction), as evidenced in Fig. 1(b) by the strong variation of contrast in the middle of the film and parallel to the interfaces. This wall takes place between *c*-like domains with opposite polarization direction induced by interfacial dipoles, in the top and bottom parts of the film, respectively, and it is similar to previous reports in ultrathin BaTiO₃ films.²⁶ In Fig. 1(c), the horizontal dark-field image shows periodic variations of contrast inclined at 45° with respect to the surface, which correspond to an *a/c* ferro-elastic/electric domain structure. The analysis of the strain fields (see [supplementary material](#), Fig. S1) has shown in-plane and out-of-plane strain variations at those 45° inclined domain walls. On the other hand, no additional strain was detected at the horizontal domain wall, confirming that the 180° horizontal domain wall is indeed purely ferroelectric. The overall polarization configuration in the film is shown schematically in Fig. 1(d).

The polarization-voltage (hysteresis) loop measured along the out-of-plane direction of the film [Fig. 2(a)] gives a saturation polarization of 25–30 $\mu\text{C}/\text{cm}^2$, similar to bulk BaTiO₃ (which is expected for this nearly zero-strain state²⁷). However, the loop shows no remanence, and the corresponding switching currents are wide and consist of two switching current peaks in each direction, instead of the one peak in each direction typically found for regular ferroelectric switching. This is consistent with the polarization switching of the two sublayers with up and down *c*-polarization, separated by the 180° domain wall observed in Fig. 1. At zero field the two sublayers possess opposing *c*-polarizations, and under a field of ± 0.1 V (10 kV/cm, see also [supplementary material](#), Fig. S2), the polarization switches to a parallel configuration. During this process, the electromechanical coupling is strong with a measured piezoelectric coefficient of $d_{33} = 70$ pm/V. This d_{33} value is larger than that of typical BaTiO₃ epitaxial films²⁸ (as they are subjected to clamping²⁹) and comparable to that of PZT or PMN-PT epitaxial films around the MPB^{30,31} or BaTiO₃ bulk single crystals.³²

When the films are grown with asymmetric electrodes (a thin SrRuO₃ or platinum electrode), the horizontal 180° charged domain wall is moved away from the center of the film, close to the surface [Figs. 1(e) and 1(f)]. Concomitantly, the ferroelectric hysteresis loop also changes drastically [Fig. 2(b)]. The switching current loop now

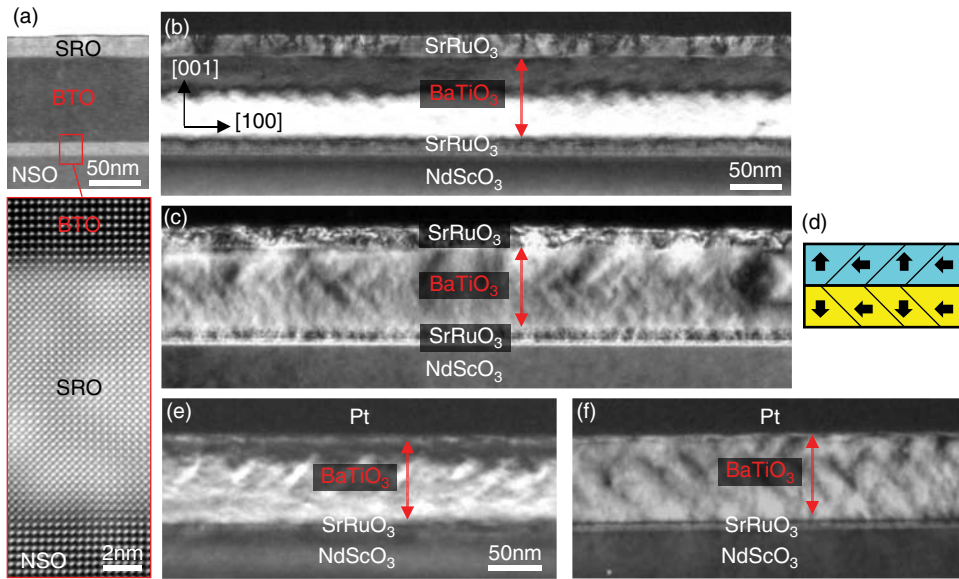


FIG. 1. (a) High resolution scanning transmission electron microscopy with a high angle annular dark-field detector (STEM-HAADF) image of an 80 nm thick BaTiO₃ film with a 12 nm SrRuO₃ bottom electrode and a 20 nm SrRuO₃ top electrode (the quasisymmetric electrode configuration). The bottom image shows a magnified view of the NdScO₃/SrRuO₃/BaTiO₃ interfaces, which shows a defect-free epitaxial growth. (b) Vertical (002) dark-field TEM images of the previous sample, which shows a strong variation of contrast in the middle of the film, attributed to a charged 180° domain wall. (c) Horizontal (200) dark-field image that shows repeated variations of contrast at 45° to the interfaces, attributed to a/c (or 90°) twin domains. (d) Simplified schematics of the domain structure and polarization directions. The cyan region represents the averaged up-polarized, and the yellow the down-polarized state, as from the vertical dark-field. (e) Vertical (002) and (f) Horizontal (200) dark-field images of an 80 nm thick BaTiO₃ film with a (reduced) 6 nm SrRuO₃ bottom electrode and a 300 nm thick Pt top electrode (the asymmetric electrode configuration).

shows a single switching current peak with an internal bias of 0.15 V (20 kV/cm). In addition, a finite remnant polarization at zero field is now present, corresponding to the imbalance of up and down polarization induced by the asymmetric configuration (see also [supplementary material](#), Fig. S3). The piezoelectric loop displays the same internal bias as the ferroelectric hysteresis and shows increased d_{33} values of 100 pm/V at the bias, or switching field, showcasing a highly asymmetric structure. Moreover, the films act as a “strain diode”³³ as there is a significant difference between the piezoelectric constant at large positive (70 pm/V) and negative (20 pm/V) biases. In this case

the effect is caused by the asymmetry of the electrodes, rather than by combining opposing ferroelectric and flexoelectric effects.

TEMPERATURE-INDEPENDENT GIANT DIELECTRIC PERMITTIVITY

When the polarization is measured in the in-plane direction, a symmetric, squared, ferroelectric hysteresis loop, similar to that of high-quality single crystals, is obtained [see Fig. 3(a)]. This loop reflects the high crystalline quality of the films with a remnant polarization of $\sim 12 \mu\text{C}/\text{cm}^2$, in agreement with the amount of

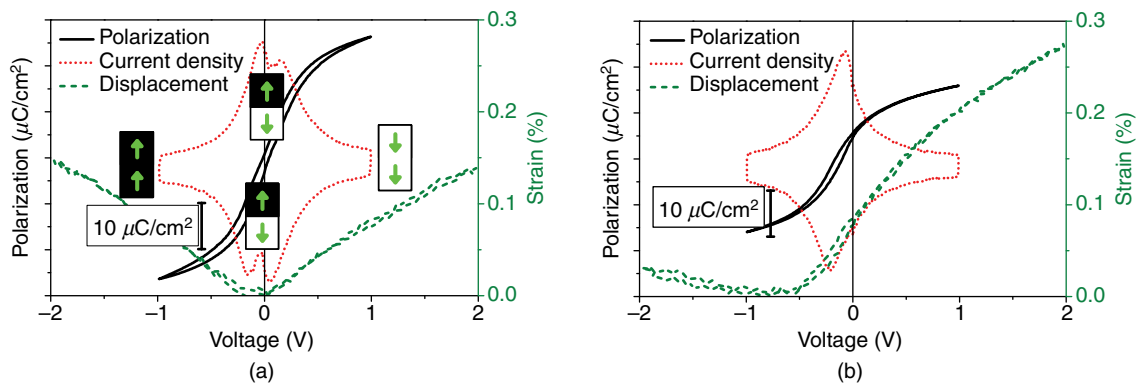


FIG. 2. (a) An 80 nm BaTiO₃ thin film with quasisymmetric 12 nm bottom and 20 nm SrRuO₃ top electrodes measured at room temperature for a 100 Hz electric field applied along the [001] out-of-plane direction. The insets show a sketch of the local averaged polarization above and below the original 180° horizontal domain wall. (b) BaTiO₃ film with asymmetric 6 nm SrRuO₃ bottom and 20 nm SrRuO₃ top electrodes. Note that the measurement technique can only measure differences in polarization.

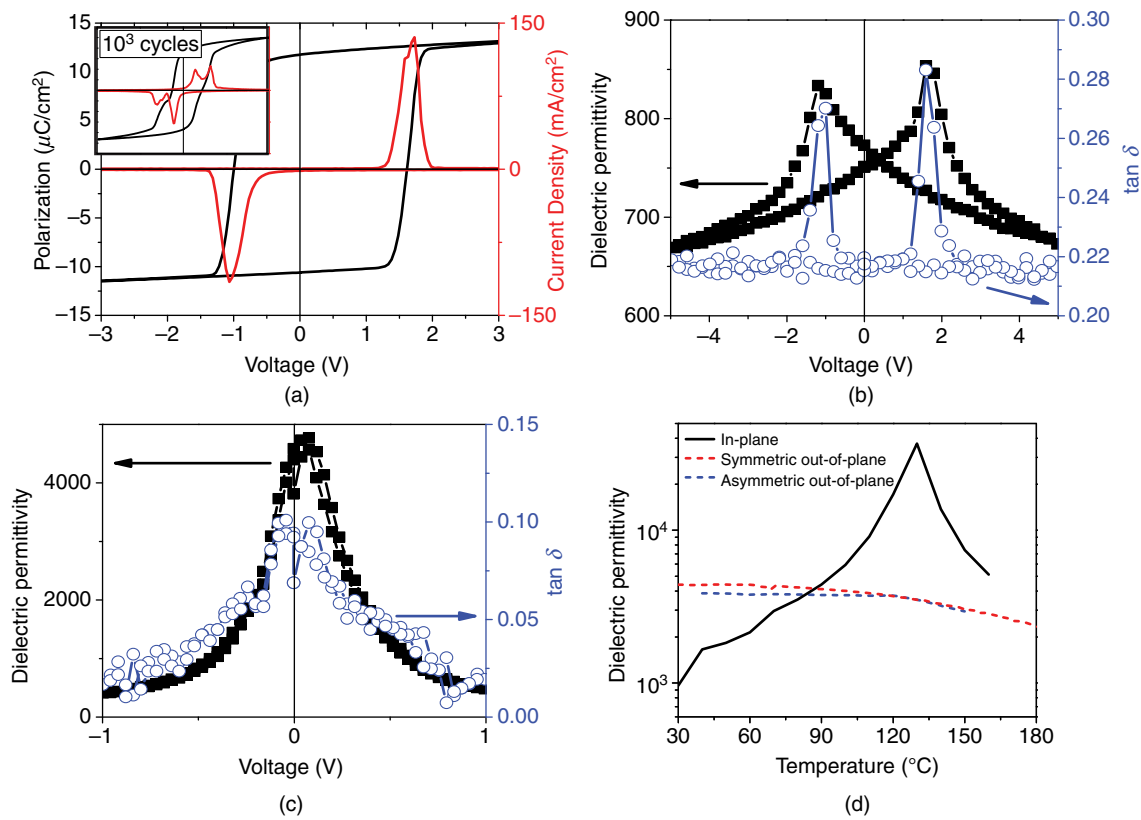


FIG. 3. (a) Ferroelectric hysteresis loop for an 80 nm film at room temperature for a 100 Hz electric field along the [100] in-plane direction with 20 nm SrRuO₃ top electrodes (with 5 μm spacing) and no bottom electrode, after 10^6 cycles. The inset shows the loop after 10^3 cycles. (b) In-plane dielectric permittivity and loss factor ($\tan \delta$) along [100] at a field frequency of 1 kHz and a small-signal voltage of 50 mV. (c) Out-of-plane (so along [001]) dielectric permittivity and loss factor ($\tan \delta$) at 1 kHz and a small-signal voltage of 50 mV using an 80 nm BaTiO₃ film with quasisymmetric 12 nm bottom and 20 nm top SrRuO₃ electrodes. (d) Dielectric permittivity for 80 nm BaTiO₃ films as a function of temperature at a DC bias of 0 V at 1 kHz for the in-plane (black) and out-of-plane directions, red for quasisymmetric electrodes and blue for asymmetric electrodes. The y-axis is in $\log(10)$ scale.

a-polarization in these *a/c* structures.¹⁹ Interestingly, these properties are only observed after field cycling, needed to remove pinched dipoles^{34,35} (as shown in [supplementary material](#), Fig. S5). The in-plane dielectric permittivity and loss value ($\tan \delta$) [Fig. 3(b)] are also typical for a ferroelectric material of excellent crystal quality, showing sharp switching signatures at the coercive field. In contrast, the dielectric permittivity along the out-of-plane direction (see also [supplementary material](#), Fig. S4) shows giant values, significantly larger than predicted for such films,²⁰ with low losses, as observed in Fig. 3(c) (see also [supplementary material](#), Fig. S6, for additional details).

In addition, the in-plane dielectric permittivity as a function of temperature [Fig. 3(d)] shows a pronounced divergence (it reaches $>25\,000$), as expected for ferroelectric crystals when approaching the ferroelectric-to-paraelectric phase transition ($T_C \sim 130^\circ\text{C}$)¹⁹ and, thus, denoting a large degree of ordering; while the out-of-plane dielectric permittivity is remarkably stable under temperature variations and only changes (decreases) significantly above T_C . The value of this out-of-plane dielectric permittivity is comparable to that of BaTiO₃ single crystals at room temperature.³⁶ However, while in BaTiO₃ single crystals, the dielectric permittivity shows a strong temperature dependence, in the present case we show a giant temperature-independent dielectric

permittivity, which—to the best of our knowledge—is larger than any of the temperature-independent dielectric permittivities reported for epitaxial thin films.^{8,10,37–39}

Vertical gradients

For a detailed understanding of the remarkable properties observed for these BaTiO₃ thin films along the out-of-plane direction, a closer look into the local structure of the films is needed. The films with dissimilar electrodes [Fig. 4(a)] provide the opportunity to explore the local strain state across the film thickness unhindered by the horizontal 180° charged domain walls. A thick 320 nm BaTiO₃ film is used to increase the dimensions of the different phases that develop across the film thickness as strain relaxes. Figure 4(b) shows a bright-field TEM image that displays 45° inclined *a/c* domains. However, the domain wall contrast disappears, gradually, toward the bottom interface [Figs. 4(c) and 4(d)]. Local TEM polarization mapping, using scanning convergent beam electron diffraction (SCBED),^{40–42} has been performed to understand the crystal symmetries involved [Fig. 5(a)]. Excellent agreement between the experiments [Figs. 5(b), 5(d), and 5(e)], and the simulated crystal symmetries [Figs. 5(c) and 5(f)],

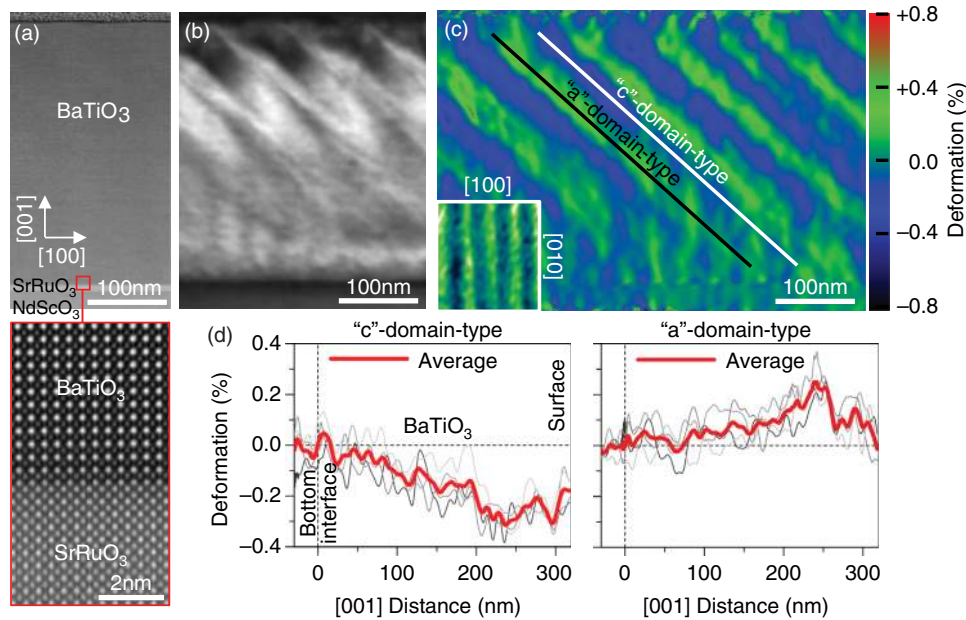


FIG. 4. (a) Aberration-corrected STEM-HAADF (scanning transmission electron microscopy with a high angle annular dark-field detector) image of a 320 nm BaTiO₃ film grown on a NdScO₃ substrate with a 6 nm SrRuO₃ electrode and a thick Pt top electrode. (Top) low magnification image of the film and (bottom) high resolution image of the SrRuO₃/BaTiO₃ interface, which shows well-defined atomic columns and a defect-free crystal lattice. (b) Bright-field TEM image of the full film along the [010] direction showing some domain contrast. (c) In-plane deformation (E_{xx}) map obtained by dark-field electron holography, showing [101] domain walls in the BaTiO₃ film. E_{xx} is defined with respect to the substrate lattice parameter. The inset in the bottom left corner shows a Piezoelectric Force Microscopy (amplitude) image of the a/c domain structure at the sample surface (viewed along the [001] direction). (d) Deformation profiles extracted from the dashed regions in (c) running in the [101] direction and plotted as a function of the distance to the bottom electrode (along [001]), at both “c”-domain-type (left) and “a”-domain-type (right), as defined by their polarization near the surface. The plots show the profiles of four distinct domains of each type (gray lines), as well as their average (red lines).

evidence distinctly different regions across the films: at the top of the film, polarization vectors along [100]/[001] are consistent with tetragonal a/c domains [Figs. 5(b) and 5(c)]. At the bottom area of the film, the domains have orthorhombic symmetry, with polar vectors along [101]/[101] [Figs. 5(e) and 5(f)]. In the middle of the layer, there exists a complex transition region with reduced symmetry [Fig. 5(d)], which cannot be reproduced in simulations, using either tetragonal or orthorhombic structure models. These monoclinic or triclinic (this distinction cannot be made in this 2D representation) lower symmetry regions seen in the SCBED are not caused by averaging over multiple nanodomains,⁴³ revealing a true low-symmetry state. These observations are in agreement with the strain analysis of Figs. 4(c) and 4(d). Here, dark-field electron holography⁴⁴ was used to measure the strain because it provides a large field of view (about $400 \times 600 \text{ nm}^2$), which allows us to map the whole film. The map and strain profiles reveal strong strain gradients that increase from the bottom interface to the top surface. The rather homogeneous strain at the bottom of the film [Fig. 4(c)] is consistent with [101]/[101] orthorhombic domains, which are indistinguishable from a strain point of view. Even though this film is significantly thicker than those used for the electrical measurements shown in Fig. 2, similar multiregion mesostructures, though with lower resolution, are found for thinner films (see supplementary material, Figs. S7 and S8). The electrical measurements of this thicker film are shown in supplementary material, Fig. S2(b). Thin films of BaTiO₃ under higher strain (on GdScO₃ substrates) have also revealed complex multiphase nanodomains.⁴⁵

To understand better the origin of the distinctly different phases found in these films, we have performed *ab initio* effective Hamiltonian calculations as well as phase-field simulations (see supplementary material Figs. S9 through S11). It is found that small changes in misfit strain ($\sim 0.01\%$) or energy ($\sim 2 \text{ meV/f.u.}$) are sufficient to stabilize either orthorhombic or tetragonal ferroelectric phases (see supplementary material Figs. S9 through S11). It is then, not unexpected to observe both types of symmetries within the same film. The need for them to coexist at the nanoscale brings intense stresses that deform the ferroelectric phases into lower symmetries and inhomogeneous structures.

TRANSITIONAL FERROELECTRIC ENABLED BY POLARIZATION ROTATION

The BaTiO₃ films reported here have remarkable properties, with wide switching current peaks, no remanent polarization, huge dielectric permittivities, and increased piezoelectric constants in the out-of-plane direction. Although some of these features may resemble relaxor materials, in this case, the BaTiO₃ films include none of the ingredients that are known to give rise to random fields or random bonds in relaxors. The in-plane measurement direction behaves like expected for a high-quality ferroelectric crystal, with a squared, large, remanent polarization hysteresis loop and a pronounced dielectric anomaly at the phase transition.

In the case of the asymmetric electrodes, along the out-of-plane direction, the strain and TEM analyses show a strain gradient, with

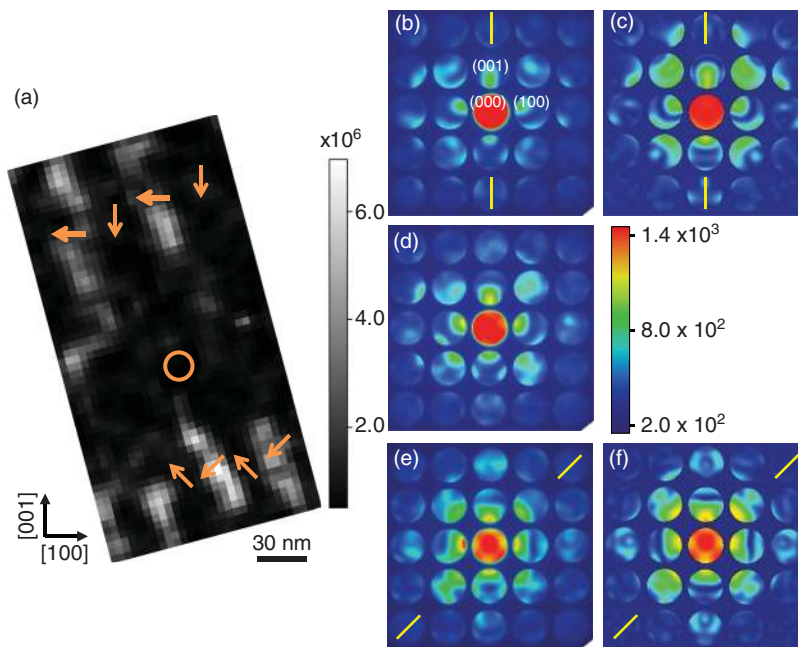


FIG. 5. (a) A 320 nm BaTiO₃ film grown on a 6 nm SrRuO₃ electrode (not visible in the figure) and a thick Pt top electrode on a NdScO₃ substrate, measured along the [010] incidence at room temperature. Image reconstructed from a SCBED dataset where the intensity is determined by the polarity of the domains. The image was obtained by comparing the intensities of four [101] reflections. Orange arrows are a sketch of specific polarization vectors obtained from local CBED patterns. (b)–(f) CBED patterns measured or simulated for different regions on the film, showcasing good agreement between measurement and simulation. The orange lines indicate the mirror plane directions, corresponding to the polarization symmetry. (b) The polarizations at the top surface correspond to tetragonal [100]/[001] polarization directions. (c) Simulated CBED pattern for the tetragonal polarizations. (d) CBED pattern corresponding to the middle part of the film (this pattern comes from the orange circle in (a), the polarization transition region). (e) and (f) Measured and simulated CBED patterns obtained in the bottom region of the film, corresponding to [101]/[101] polarization directions.

low-symmetry phases bridging the expected tetragonal and orthorhombic phases, to provide a polarization rotation coupled to the strain gradient. This low-symmetry transitional phase denotes a flat energy landscape that enables continuous polarization rotation between the tetragonal and orthorhombic phase, which is independent of temperature. The huge dielectric permittivity of >4000 originates from the easy rotation of the polarization even for small fields (see [supplementary material](#), Fig. S6) due to the continuous polarization rotation mechanism. Similar materials with a polarization gradient but without polarization rotation^{10,46} or BaTiO₃ films without low-symmetry phases^{27,47} do not show such temperature-independent response.

The quasisymmetric electrode configuration shares these functional properties related to the low-symmetry phase, namely wide switching current peaks, increased piezoelectric d_{33} coefficient, and huge temperature-independent dielectric permittivity, with the asymmetric case, as observed in Fig. 2. The internal bias in the asymmetric configuration is created by uncompensated dipoles [as easily seen in Fig. 5(a)] to create the asymmetric structure, leading to a strain diode, while in this quasisymmetric configuration, the 180° domain wall in the center compensates those two sets of dipoles with two switching peaks to get an effective zero internal bias and more symmetric structure.

Some of the properties of this material resembles those of morphotropic phase boundaries (MPBs), in PbZr_xTi_{1-x}O₃ (PZT) and the ferroelectric relaxors solid solutions, as well as those of BaTiO₃ crystals at the thermotropic phase boundary¹⁷ or BaTiO₃ engineered

nanodomains.⁴⁸ In addition, strain,¹⁸ stress,⁴⁹ or electron beam radiation⁴⁸ can create multiple phases, multidomains, and “ferroelectric-glass” states⁴⁸ that share some similar features with MPB systems, which have been shown to display bridging phases at the boundary between two or more phases and to exhibit rotational degrees of freedom with an enhancement of the dielectric permittivity/piezoelectric response. However, not all these systems can be engineered such that the coexistence region and bridging phases are weakly dependent of temperature (a key ingredient for their utilization in devices). The BaTiO₃/NdScO₃ system fulfills this condition and stays in such intermediate, or transitional, state in a wide temperature range, similar to the MPB ferroelectrics. Nevertheless, microscopically, the material is clearly different since it cannot be considered a polycrystal but also not a single crystal, and it is not a relaxor but also not a homogeneous ferroelectric. The microstructure of the material presented here is closer to the compositionally graded ferroelectrics, but in this case, the grading is strain-mediated and self-organized naturally during the material processing. Thus, it seems appropriate to use a broader term to refer to materials that exist in an intermediate, or coexisting, state that is robust against temperature variations. We propose to coin these materials as “transitional ferroelectrics.”

Concluding, this work demonstrates that transitional states, enabled by polarization rotation gradients and engineered by utilizing materials with nearly degenerate, differently oriented polar phases have properties that are distinct from those of single crystals, multidomain crystals, ceramics, or relaxor ferroelectrics. We show that, in

BaTiO₃ thin films grown on NdScO₃ substrates with varying thicknesses of SrRuO₃ electrodes, these gradients facilitate an electrical-field-induced gradual rotation of the polarization. While the in-plane direction shows standard ferroelectric behavior, the out-of-plane direction shows a flat energy landscape. It manages to achieve a giant dielectric permittivity with a large piezoelectric constant as would be characteristic of MPBs, while managing an exceptional temperature-stability without requiring demanding boundary conditions. This combination of properties enables energy-efficient electromechanical functionalities and represents the dielectric equivalent of a magnetic Permalloy with high permittivity that is largely temperature-independent and with dielectric hard and easy axes. Similar mechanisms could be utilized in the design of other low power ferroelectrics, piezoelectrics, dielectrics, or shape-memory alloys, as well as in efficient electro- and magnetocaloric cooling.

SUPPLEMENTARY MATERIAL

See the [supplementary material](#) for details on the experimental methods, *ab initio* effective Hamiltonian calculations and phase-field simulations (Note S1); additional STEM-HAADF on a 80 nm thick BaTiO₃ film (Note S2, Fig. S1); additional ferroelectric and dielectric measurements (Note S3, Fig. S2); differently biased ferroelectric loops depending on the electrode configuration (Note S4, Fig. S3); effect of the number of cycles on the out-of-plane ferroelectric switching (Note S5, Figs. S4 and S5); small signal ferroelectric measurements (Note S6, Fig. S6); additional SCBED measurements (Note S7, Figs. S7 and S8). In Note S8, the theoretical results are included in the form of both *ab initio* effective Hamiltonian calculations (Figs. S9 and S10) and phase-field simulations (Fig. S11).

ACKNOWLEDGMENTS

The authors are grateful to U. Bhaskar for preliminary piezoelectric measurements, to C. Magén for preliminary TEM measurements, to G. Agnus for developing oxides patterning processes, and to N. Robin, P. Murali, and D. Damjanovic for useful discussions. A.S.E. and B.N. acknowledge financial support from the alumni organization of the University of Groningen, De-Aduarderking (Ubbo Emmius Fonds), and from the Zernike Institute for Advanced Materials. T.D. acknowledges the European Metrology Research Programme (EMRP) Project No. IND54 397 Nanostrain and the European Union's Seventh Framework Programme (No. FP7/2007-2013)/ERC Grant Agreement No. 320832. T.D. thanks Knut Müller-Caspary for technical help with the STEM experiment. A.G. acknowledges funding by the Deutsche Forschungsgemeinschaft (Nos. SPP 1599 GR 4792/1-2 and GR 4792/2-1). Y.T.S. and J.M.Z. acknowledge the financial support by the DOE BES (Grant No. DEFG02-01ER45923). Electron diffraction experiments were carried out at the Center for Microanalysis of Materials at the Frederick Seitz Materials Research Laboratory of the University of Illinois at Urbana-Champaign. J.H. and P.O. were supported by the Operational Programme Research, Development, and Education (financed by European Structural and Investment Funds and by the Czech Ministry of Education, Youth, and Sports), Project No. SOLID21-CZ.02.1.01/0.0/0.0/16_019/0000760). N.D. and G.C. acknowledge financial support by the Severo Ochoa Excellence programme.

REFERENCES

- ¹K. G. Wilson, *Phys. Rev. B* **4**, 3174 (1971).
- ²M. E. Lines and A. M. Glass, *Principles and Applications of Ferroelectrics and Related Materials* (Oxford University Press, Oxford, 1977).
- ³D. B. Strukov, G. S. Snider, D. R. Stewart, and R. S. Williams, *Nature* **453**, 80 (2008).
- ⁴F. Weyland, M. Acosta, J. Koruza, P. Breckner, J. Rödel, and N. Novak, *Adv. Funct. Mater.* **26**, 7326 (2016).
- ⁵S. H. Baek, J. Park, D. M. Kim, V. A. Aksyuk, R. R. Das, S. D. Bu, D. A. Felker, J. Lettieri, V. Vaithyanathan, S. S. N. Bharadwaja, N. Bassiri-Gharb, Y. B. Chen, H. P. Sun, C. M. Folkman, H. W. Jang, D. J. Kreft, S. K. Streiffer, R. Ramesh, X. Q. Pan, S. Trolier-McKinstry, D. G. Schlom, M. S. Rzchowski, R. H. Blick, and C. B. Eom, *Science* **334**, 958 (2011).
- ⁶Z. Luo, D. Zhang, Y. Liu, D. Zhou, Y. Yao, C. Liu, B. Dkhil, X. Ren, and X. Lou, *Appl. Phys. Lett.* **105**, 102904 (2014).
- ⁷W. J. Merz, *Phys. Rev.* **91**, 513 (1953).
- ⁸P. Zubko, N. Jecklin, N. Stucki, C. Lichtensteiger, G. Rispens, and J.-M. Triscone, *Ferroelectrics* **433**, 127 (2012).
- ⁹M. Acosta, N. Novak, V. Rojas, S. Patel, R. Vaish, J. Koruza, G. A. Rossetti, and J. Rödel, *Appl. Phys. Rev.* **4**, 041305 (2017).
- ¹⁰A. R. Damodaran, S. Pandya, Y. Qi, S.-L. Hsu, S. Liu, C. Nelson, A. Dasgupta, P. Ercius, C. Ophus, L. R. Dedon, J. C. Agar, H. Lu, J. Zhang, A. M. Minor, A. M. Rappe, and L. W. Martin, *Nat. Commun.* **8**, 14961 (2017).
- ¹¹S. E. Park and T. R. ShROUT, *J. Appl. Phys.* **82**, 1804 (1997).
- ¹²R. Guo, L. E. Cross, S.-E. Park, B. Noheda, D. E. Cox, and G. Shirane, *Phys. Rev. Lett.* **84**, 5423 (2000).
- ¹³L. Bellaiche, A. García, and D. Vanderbilt, *Phys. Rev. Lett.* **84**, 5427 (2000).
- ¹⁴H. Fu and R. E. Cohen, *Nature* **403**, 281 (2000).
- ¹⁵M. Davis, M. Budimir, D. Damjanovic, and N. Setter, *J. Appl. Phys.* **101**, 054112 (2007).
- ¹⁶Y. M. Jin, Y. U. Wang, A. G. Khachatryan, J. F. Li, and D. Viehland, *Phys. Rev. Lett.* **91**, 197601 (2003).
- ¹⁷T. T. A. Lummen, Y. Gu, J. Wang, S. Lei, F. Xue, A. Kumar, A. T. Barnes, E. Barnes, S. Denev, A. Belianinov, M. Holt, A. N. Morozovska, S. V. Kalinin, L.-Q. Chen, and V. Gopalan, *Nat. Commun.* **5**, 3172 (2014).
- ¹⁸R. J. Zeches, M. D. Rossell, J. X. Zhang, A. J. Hatt, Q. He, C.-H. Yang, A. Kumar, C. H. Wang, A. Melville, C. Adamo, G. Sheng, Y.-H. Chu, J. F. Ihlefeld, R. Erni, C. Ederer, V. Gopalan, L. Q. Chen, D. G. Schlom, N. A. Spaldin, L. W. Martin, and R. Ramesh, *Science* **326**, 977 (2009).
- ¹⁹A. S. Everhardt, S. Matzen, N. Domingo, G. Catalan, and B. Noheda, *Adv. Electron. Mater.* **2**, 1500214 (2016).
- ²⁰V. G. Koukhar, N. A. Pertsev, and R. Waser, *Phys. Rev. B* **64**, 214103 (2001).
- ²¹A. Grünebohm, M. Marathe, and C. Ederer, *Appl. Phys. Lett.* **107**, 102901 (2015).
- ²²Y. L. Li and L. Q. Chen, *Appl. Phys. Lett.* **88**, 072905 (2006).
- ²³S. Choudhury, Y. L. Li, L. Q. Chen, and Q. X. Jia, *Appl. Phys. Lett.* **92**, 142907 (2008).
- ²⁴M. Tanaka, N. Kitamura, and G. Honjo, *J. Phys. Soc. Jpn.* **17**, 1197 (1962).
- ²⁵T. Asada and Y. Koyama, *Phys. Rev. B* **70**, 104105 (2004).
- ²⁶G. Sanchez-Santolino, J. Tornos, D. Hernandez-Martin, J. I. Beltran, C. Munuera, M. Cabero, A. Perez-Muñoz, J. Ricote, F. Mompean, M. Garcia-Hernandez, Z. Sefrioui, C. Leon, S. J. Pennycook, M. C. Muñoz, M. Varela, and J. Santamaria, *Nat. Nanotechnol.* **12**, 655 (2017).
- ²⁷K. J. Choi, M. Biegalski, Y. L. Li, A. Sharan, J. Schubert, R. Uecker, P. Reiche, Y. B. Chen, X. Q. Pan, V. Gopalan, L.-Q. Chen, D. G. Schlom, and C. B. Eom, *Science* **306**, 1005 (2004).
- ²⁸V. Thery, A. Bayart, J.-F. Blach, P. Roussel, and S. Saitzek, *Appl. Surf. Sci.* **351**, 480 (2015).
- ²⁹R. Mahjoub, S. P. Alpay, and V. Nagarajan, *Phys. Rev. Lett.* **105**, 197601 (2010).
- ³⁰A. Kholkin, M. Calzada, P. Ramos, J. Mendiola, and N. Setter, *Appl. Phys. Lett.* **69**, 3602 (1996).
- ³¹M. Boota, E. P. Houwman, M. Dekkers, M. D. Nguyen, K. H. Vergeer, G. Lanzara, G. Koster, and G. Rijnders, *Sci. Technol. Adv. Mater.* **17**, 45 (2016).
- ³²S. Wada, S. Suzuki, T. Noma, T. Suzuki, M. Osada, M. Kakihana, S.-E. Park, L. E. Cross, and T. R. ShROUT, *Jpn. J. Appl. Phys., Part 1* **38**, 5505 (1999).

- ³³U. K. Bhaskar, N. Banerjee, A. Abdollahi, G. Rijnders, E. Solanas, and G. Catalan, *Nanoscale* **8**, 1293 (2016).
- ³⁴M. I. Morozov and D. Damjanovic, *J. Appl. Phys.* **104**, 034107 (2008).
- ³⁵K. Carl and K. H. Hardtl, *Ferroelectrics* **17**, 473 (1977).
- ³⁶F. Jona and G. Shirane, *Ferroelectric Crystals* (Dover Publications, Inc., Mineola, 1993).
- ³⁷J. H. Haeni, P. Irvin, W. Chang, R. Uecker, P. Reiche, Y. L. Li, S. Choudhury, W. Tian, M. E. Hawley, B. Craigo, A. K. Tagantsev, X. Q. Pan, S. K. Streiffer, L. Q. Chen, S. W. Kirchoefer, J. Levy, and D. G. Schlom, *Nature* **430**, 758 (2004).
- ³⁸P. Gerber, C. Kügeler, U. Böttger, and R. Waser, *J. Appl. Phys.* **98**, 124101 (2005).
- ³⁹E. Bousquet, M. Dawber, N. Stucki, C. Lichtensteiger, P. Hermet, S. Gariglio, J. M. Triscone, and P. Ghosez, *Nature* **452**, 732 (2008).
- ⁴⁰K. H. Kim and J. M. Zuo, *Ultramicroscopy* **124**, 71 (2013).
- ⁴¹Y. T. Shao and J. M. Zuo, *Acta Crystallogr.* **73**, 708 (2017).
- ⁴²Y. T. Shao and J. M. Zuo, *Phys. Rev. Lett.* **118**, 157601 (2017).
- ⁴³K. Kim and J. Zuo, *Acta Crystallogr.* **A70**, 583 (2014).
- ⁴⁴M. Hÿtch, F. Houdellier, F. Hÿe, and E. Snoeck, *Nature* **453**, 1086 (2008).
- ⁴⁵S. Kobayashi, K. Inoue, T. Kato, Y. Ikuhara, and T. Yamamoto, *J. Appl. Phys.* **123**, 064102 (2018).
- ⁴⁶J. C. Agar, A. R. Damodaran, M. B. Okatan, J. Kacher, C. Gammer, R. K. Vasudevan, S. Pandya, R. V. K. Mangalam, G. A. Velarde, S. Jesse, N. Balke, A. M. Minor, S. V. Kalinin, and L. W. Martin, *Nat. Mater.* **15**, 549 (2016).
- ⁴⁷A. R. Damodaran, E. Breckenfeld, Z. Chen, S. Lee, and L. W. Martin, *Adv. Mater.* **26**, 6341 (2014).
- ⁴⁸R. Ahluwalia, N. Ng, A. Schilling, R. G. P. McQuaid, D. M. Evans, J. M. Gregg, D. J. Srolovitz, and J. F. Scott, *Phys. Rev. Lett.* **111**, 165702 (2013).
- ⁴⁹M. Ahart, M. Somayazulu, R. E. Cohen, P. Ganesh, P. Dera, H. K. Mao, R. J. Hemley, Y. Ren, P. Liermann, and Z. Wu, *Nature* **451**, 545 (2008).